Measuring the surface stress polar dependence

J. J Métois, A. Saul, P. Muller

Measuring the surface stress polar dependence

J.J.Métois, A.Saúl, P.Müller

Centre de Recherche sur la Matière Condensée et les Nanosciences,
CNRS, Aix-Marseille Université
Campus de Luminy, case 913, F-13288 Marseille Cedex 9, France

Abstract:

While measurements of the polar dependence of the surface free energy are easily available, measurements of the whole polar dependence of the surface stress of a crystal do not exist. In this paper is presented a new procedure that allows, for the first time, the experimental determination of the surface stress polar dependence of a crystal. For this purpose (1) electromigration is used to control the kinetic faceting of surface orientations that belong to the equilibrium shape of the crystal and (2) for each destabilised surface, the period of faceting as well as the crystallographic angles of the appearing facets are measured by AFM. The so-obtained data lead to a set of equations whose mathematical solution, compatible with physical constraints, gives access to the surface stress polar dependence of the whole crystal and thus to a better understanding of surface stress properties.

Two distinct macroscopic quantities are needed to describe the thermodynamics properties of a crystalline surface n characterized by its normal direction $\hat{n}$: the surface free energy per unit area γ^n which measures the cost of creating a surface area at constant deformation and the surface stress $[s]^n$, which measures the energy cost for deforming a surface at constant number of surface atoms. While γ^n is a positive scalar, the surface stress, which depends upon the direction of stretching, is a second rank tensor. If the surface tends to shrink (resp: expand) with respect to the bulk in one direction, the corresponding surface stress component s_{ij}^n is positive (resp: negative) and is said to be tensile (resp: compressive). Since, in vacuum, a fully relaxed surface has no normal stress, the surface stress can be simply considered as a two-dimensional tensor which, when diagonalised, is simply characterized by two orthogonal components. Because of the anisotropic nature of the crystalline state, surface stress as well as surface free energy depends upon the orientation of the crystalline surface. However while measurements of the polar plot of the surface energy (that means its dependence with the surface orientation $\hat{n}$) can be easily obtained from a detailed study of the equilibrium shape of 3D crystals[1,2] , measurements of the polar plot of the surface stress of a crystal are still lacking[3,4]. This is the most puzzling that during the last decade there has been an increasing interest to understand the influence of surface stress on

many physical properties such as surface relaxation or reconstruction[5-7], surface segregation[8], surface adsorption[9], nano-sensors properties[10] and self assembling[11,12]. Moreover, surface stress is very often the main driving force for bottom-up nanostructuration[13]. *The new procedure we propose enables for the first time the experimental determination of the surface stress polar plot of a crystal.*

Since the equilibrium shape of a free crystal is the one, which minimizes its surface free energy, it is intuitive that the geometrical description of the equilibrium shape (ES) of a crystal is an image of its surface free energy anisotropy[14] . Thus, the polar plot of the surface free energy of all the surface orientations that belong to the equilibrium shape can be obtained from a simple inverse geometrical construction (in Fig. 1 is given the Silicon ES and its corresponding γ -plot[2]). Missing orientations on the equilibrium shape (ES) correspond to unstable surfaces. If such an unstable surface is macroscopically prepared (by slicing a crystal for instance), then annealed (to equilibrate it) it breaks up into facets of the two neighboring orientations present on the equilibrium shape of the crystal[15]. The period of this spontaneous faceting is connected to the surface stress difference between the two stable orientations[11,12], which thus can be extracted from a simple wavelength measurement[16]. However, this procedure cannot be used for the crystallographic orientations that belong to the equilibrium shape which, since stable, do not facet upon annealing and thus, give no information on surface stress. Nevertheless, we show that this problem can be get round each time it is possible to use an external constraint to destabilize these stable surfaces. It is in particular the case of the stable vicinal faces of W[17], Ta, Mo, Pt, Fe, Ni[18] and Si[19], which can be destabilized by adatom migration leading to a step bunching instability and then to kinetic faceting[19-23]. *In this work, such electromigration driving force is used to destabilize some well-chosen vicinal facets in order to obtain the surface stress anisotropy of all the directions that belong to the equilibrium shape.* Because of its technological importance we have chosen silicon for which a good knowledge of the surface stress anisotropy should be welcomed!

For our purpose, we have selected the (118), (223) (443) and (105) stable vicinal faces (whose orientations were controlled by Laue diffraction) of a Silicon crystal (Fig. 2) and heated them, in ultra high vacuum conditions, by Joule effect (AC or DC current). Since at 1423 K the evaporation rate is of 0.02 bilayer per second, a clean surface is thus periodically regenerated avoiding any foreign adsorption as confirmed by the absence of pinning points in the AFM images even after several hours at 1423 K. When using AC current, all the vicinal surfaces

remain flat, while using DC current, in the direction of ascending steps (that means in the $[44\bar{1}]$, $[33\bar{4}]$, $[33\bar{8}]$, and $[\bar{1}50]$directions for the (118), (223), (443) and (510) surfaces respectively) in the range 1200-1400K, the surfaces break up into a hill-and-valley structure (Fig. 3)[19-21]. There is no faceting with DC current in the direction of descending steps.

A further annealing by AC current of the so-facetted structure restores the flatness of the nominal vicinal face. The physical interpretation is clear: with the AC current, the electromigration-driven instability no more works and the Joule effect restores the original stable vicinal face initially obtained by mechanical slicing. It thus confirms that the faceting we observe is a kinetic effect due to adatom drift induced by the electrical field[21-23].

In Fig. 4 we show, for each vicinal surface, the time evolution of the faceting period and of the angle β that one of the facets of the hill-and-valley structure forms with the nominal orientation. The angle α of the other facet does not vary with time. (α and β are shown on Fig. 5). The following results are worth to be underlined.

1/ The period and the orientation of the so-formed facets evolve with time. After several hundred hours of annealing, a steady-state structure formed by the so-called facets F_1 and F_2 is reached. As schematically shown in Fig. 5, the facet F_1 is already present in the original vicinal surface so that its area simply increases with time at constant angle α while the facet F_2 slowly builds by step bunching (the angle β and the facet area thus increase with time). In Table I we report the vicinal Si faces that we have chosen and the corresponding facets F_1 and F_2 whose crystallographic indexes have been obtained from the measurement of α and β.

2/ For Silicon, the facets F_1 and F_2 correspond to cusps on the free energy polar plot (Fig. 1). More precisely, they correspond to the two closest facets in the equilibrium shape surrounding the original vicinal face (Fig. 2).

The importance of elastic effects in periodic faceting kinetics has been recognized long time ago[11,12]: the longest wavelengths originate from elastic interactions, while the shorter ones may have a pure kinetic origin[24,25]. In the particular case of Si annealed at 1213 K, Song et al.[26,27] have determined the position of the crossover between both mechanisms. For Si(113), they have found that the weaker periods ($L<10^3$ Å for time $t<10^3$ s) follow a power-law versus time characteristic of a zipping mechanism (in which two separate bunches zip each other to form a bigger bunch), while the longer ones asymptotically reach a state where elasticity plays

the major role for t≈10^4 s and L≈1.310^3 Å. In our experiments, at higher temperature, the steady state is obtained after roughly 10^6 to 10^7s where the so-obtained periods are of the order of microns. So, the intermediate states (before the asymptote) reported in Fig. 4 are located after the crossover and thus belong to the elastic range. In conclusion, taking into account the propagation of the elastic interaction (at the sound velocity), the fast surface diffusion that occurs at 1373 K, and that the periods (~ 4μm) of these intermediate states are much closer to the final periodic structure (~ 10μm) than to the original step distance of the vicinal orientation (~ 10Å), we believe that a local chemical equilibrium is achieved at each step of the process.

In equilibrium conditions, the elastic origin of the periodicity has been established by Marchenko and Alerhand et al.[11,12]. When two facets a and b (characterized by their normal directions $\hat{n}_a$ and $\hat{n}_b$ and their surface stress tensors $[s]^{n_a}$ and $[s]^{n_b}$) have a common edge (characterized by its tangential unit vector $\hat{\tau}$), at the boundary between both facets exists an elastic force $\vec{f} = \vec{s}_\tau^{\,n_a} - \vec{s}_\tau^{\,n_b}$, where $\vec{s}_\tau^{\,n_a} = [s]^{n_a}\left(\hat{\tau} \wedge \hat{n}_a\right)$ is the force per unit length across the common edge boundary (Fig. 2 and Fig. 5 for t=t_2 and t→∞). This localized force deforms the underlying bulk and thus decreases the total energy by means of stress relaxation. The periodicity results from a competition between the positive edge energy ρ and the negative stress relaxation. More precisely the wavelength reads[11,12]:

$$\lambda = \frac{2\pi c}{\sin \pi\theta} \exp\left(1 + \frac{\pi E \rho}{2 f^2 \left(1-\nu^2\right)}\right) \qquad \textbf{(1)}$$

where E and ν are respectively the Young modulus and the Poisson ratio of the material (calculated for the good crystallographic orientations), c an atomic unit,

$f^2 = \left(s_\tau^{n_a} - s_\tau^{n_b}\right)^2 + 4 s_\tau^{n_a} s_\tau^{n_b} \sin^2\left(\frac{\alpha+\beta}{2}\right)$ where α and β are the angles the faces a and b form with the original orientation (Fig. 5), and $\theta = \frac{tg\alpha}{tg\alpha + tg\beta}$ a geometrical factor. For a given facetted system the angles α and β can be measured so that, for a fixed value of the edge energy ρ, the period $\lambda\left(\alpha, \beta, s_\tau^{n_a}, s_\tau^{n_b}\right)$ only depends upon the unknown values $s_\tau^{n_a}$ and $s_\tau^{n_b}$.

Since surfaces having a symmetry axis greater than two have isotropic surface stresses and owing to the chosen vicinal orientations (with common zone axis as for example (118) and

(223) faces in Fig. 2.), the set of periods of the vicinal faces that we have considered only depends upon five unknown quantities: $s_{\bar{1}10}^{001}$, $s_{\bar{1}10}^{113}$, $s_{\bar{1}10}^{111}$, $s_{\bar{1}10}^{110}$ and the anisotropic factor χ defined by $s_{\bar{1}10}^{110} = s_{001}^{110}(1+\chi)$. Thus measuring (by AFM) the periods and the angles α and β of a set of completely destabilized vicinal faces (labeled k) is enough to obtain a system of equations $\lambda^k\left(\alpha^k, \beta^k, s_{\tau_k}^{n_{a_k}}, s_{\tau_k}^{n_{b_k}}\right)$ that can be numerically solved to obtain all the unknown quantities. Moreover, the hypothesis of local equilibrium enables us to use some of the other intermediate states (before the final asymptote but far away the crossover) whose facet orientations are simply determined by the angle they form with the mean face, to calculate the surface stress of the intermediate surface orientations. However, only some of the many numerical solutions of the system have a physical meaning. In particular, we consider two important physical constraints. Firstly, close to a low index orientation, step creation has an energetic cost but allows relaxing the surface stress so that a face that belongs to the equilibrium shape is a minimum of surface energy but a maximum of surface stress[4]. Secondly, to the best of our knowledge, surface stresses of clean reconstructed surfaces are known to be positive[3,4,28]. We find a single numerical solution, which verifies both physical constraints. It corresponds to a negative anisotropy factor ($\chi = -0.40 \pm 0.05$) quite consistent with the structure of the Si(110) surface[29]. The corresponding surface stress plot given in Fig. 6 is calculated for a constant value of ρ but the introduction of reasonable edge energy anisotropy (20%) does not affect substantially the surface stress plot. Notice that because of the tensorial nature of the surface stress, two branches are necessary to represent the surface stress anisotropy of the two perpendicular components s_τ^n and s_ω^n (where $\hat{\omega} = \hat{t} \wedge \hat{n}$ is the unit vector normal to the edge). However, the procedure we describe only gives access to the s_τ^n component (perpendicular to the common edge τ of the facets), that means between $[001]$ and $[110]$ directions to $s_{1\bar{1}0}^n$ and between $[110]$ and $[100]$ directions to s_{001}^n (Fig. 2). Obviously for the anisotropic (110) surface we thus have access to the two orthogonal components $s_{1\bar{1}0}^{110}$ and s_{001}^{110} of the surface stress tensor $[s]^{110}$. The so-obtained surface stress values, connected by a continuous line (simple guide for the eyes) are plotted on Fig. 6.

Let us comment some interesting points:

(1) Since in the common direction $\hat{\tau}$ (Fig. 2) all the surfaces exhibit more or less the same local step geometry (dense row) while in the orthogonal direction $\hat{\omega}$ the local geometry of the microfacets formed by the step and the underneath terrace varies a lot, the

surface stress anisotropy cannot have the same amplitude for the two branches of the surface stress plot. In other words the s_τ^n anisotropy must always be larger than the s_ω^n one, so that our procedure gives access to the polar plot of the more anisotropic branch of surface stress that means here to $s_{1\bar{1}0}^n$ anisotropy between $[110]$ and $[100]$ directions and to s_{001}^n anisotropy between $[001]$ and $[110]$ directions (Fig. 6).

(2) The surface stress anisotropy is more important than the surface energy anisotropy (compare the scales of Fig. 1 and 6). This behaviour is quite normal since it is well known that surface stress is much more sensitive to surface relaxation than surface energy[4].

(3) Open surfaces relax easier than dense ones and thus exhibit smaller surface stress. It is the case of the (113) surface in comparison to the (111) or (001) surfaces.

(4) Our procedure does not give access to the polar plot of the weak anisotropic branch (see point (1)). Nevertheless the surface stress anisotropy calculated for several materials[4] can be used to estimate a zone in which should appear this branch s_ω^n. For this purpose we simply draw (in grey in Fig. 6) a zone in which should lie the less anisotropic branches calculated for most of these materials. However, since calculations can hardly take into account at the same time the complex surface reconstructions, surface relaxations and the important entropic effects, a detailed comparison remains difficult.

(5) Since the kinetic pathway towards the two closest facets F_1 and F_2 are very different, the decomposition of the original vicinal surface only gives access to the surface stress of the intermediate orientations which are close to the facet having the slowest kinetics (here F_2). Thus the experimental branch is incomplete in the vicinity of the F_1 surface. More precisely, a vicinal (111) surface gives access to the stress variation near (110) or (113) orientation but not near the (111) orientation. At the same time, a vicinal surface of the (100) orientation only gives information on surface stress variations near (110) or (113) but not near (100) (Fig. 6). Thus in order to "fill the holes" of the polar plot one must use other vicinal faces: a vicinal of (113) to get the surface stress change near (111) or (001) orientations and a vicinal of (110) to get the surface stress change near (111) and (100) orientations. Unfortunately, one encounters in these cases a new experimental problem related with the fact that it is easier to reach a stepped face by the step bunching mechanism than to reach a flat surface for which supplementary activation energy for step coalescence is needed. It is for this reason that using a vicinal (113) face we couldn't explore an angular domain greater than 8°

near the (111) or (100) surface, even after 15 days of annealing at 1373K, as already depicted by Song et al.[26,30].

In summary, we have shown that the control of kinetic faceting induced by adatom electromigration enables, for the first time, to determine the surface stress polar dependence of stable facets belonging to the equilibrium shape. The procedure that we propose can be extended to other materials for which (i) the orientations that belong to the equilibrium shape (surface energy plot) are known, (ii) a controlled mechanism for faceting (electromigration or any other) exists, and (iii) working at high temperature and for a long time is possible. It is not difficult to find materials for which these conditions apply. For example, (i) the equilibrium shape of Au, In, Pb, Cu… has been already determined experimentally, (ii) electromigration driven faceting has been recognized to work for many metals including W, Ta, Mo, Pt, Ni… and (iii) a rough indicate of what high temperature means, is T between $2/3T_m$ and T_m with T_m the melting point in order to insure a great enough diffusion.

References:

1. Sundquist, B. A direct determination of the anisotropy of the surface energy of solid Au, Cr, Ni, α-Fe. *Acta. Metall.* **12** 67-86 (1964).
2. Bermond, J.M., Métois, J.J., Egea X. & Floret F. The equilibrium shape of silicon. *Surf. Sci.* **330** 48-60 (1995).
3. Ibach, H. The role of surface stress in reconstruction, epitaxial growth and stabilization of mesoscopic structures. *Surf. Sci. Rep.* **29** 193-263 (1999).
4. Müller, P. & Saùl, A. Elastic effects on surface physics. *Surf. Sci. Rep.* **54** 157-258 (2004) .
5. Bach, C., Giesen, M., Ibach, H. & Einstein, T. Stress relief in reconstruction. *Phys. Rev. Lett.* **78** 4225-4228 (1997).
6. Filipetti, A. & Fiorentini, V. Faceting and stress of missing-row reconstructed transition-metal (110) surfaces. *Surf. Sci.* **377** 112-116 (1997).
7. Olivier, S., Saúl, A. & Tréglia, G. Relation between surface stress and (1x2) reconstruction for (110) fcc transition metal surfaces. *Appl. Surf. Sci.* **212/213** 866-871 (2003).
8. Wynblatt, P. & Ku, R. Surface energy and solute strain energy effects in surface segregation. *Surf. Sci.* **65** 511-531 (1977).
9. Ibach, H. The relation between the strain-dependence of the heat of adsorption and the coverage dependence of the adsorption induced surface stress. *Surf. Sci.* **556** 71-77 (2004).
10. Berger, R. *et al.* Surface stress in the self-assembly of alkanethiols on gold. *Science* **276** 2021-2024 (1997).
11. Marchenko, V. Theory of the equilibrium shape of crystals. *JETP* **54** 605-607 (1981).
12. Alerhand, O. Vanderbilt, D., Meade, R. & Joannopoulos J. Spontaneous formation of stress domains on crystal surfaces. *Phys. Rev. Lett.* **61** 1973-1976 (1988).
13. Rousset, S. *et al.* Self-ordering on crystal surfaces: fundamentals and applications. *Mat. Sci. And Eng.* B **96** 169-177 (2002).

14. Wulff, G. Zur frage der geschwindigkeit des wachsthums und der auflösung der krystallfläschen. *Z.Kristall.* **34** 449-480 (1901).
15. Herring, C. Some theorems on the free energies of crystal surfaces. *Phys. Rev.* **82** 87-93 (1951).
16. Rousset, S. *et al.* Self-organization on Au(111) vicinal surfaces and the role of surface stress. *Surf. Sci.* **422** 33-41 (1999).
17. Johnson, R. Construction of filaments surfaces. *Phys. Rev.* **54** 459-467 (1938).
18. Moore, A. « Thermal faceting » in Metal surfaces: structure, energetics and kinetics (Ed. American Society for Metals, Metals Park, Ohio) 1962, p155.
19. Latyshev, A., Litvin L., & Aseev, A. Peculiarities of step bunching on Si(001) surface induced by DC heating. *Appl. Surf. Sci.* **130/132** 139-145 (1998).
20. Métois, J.J. & Stoyanov, S. Impact of the growth on the stability-instability transition at Si(111) during step bunching induced by electromigration. *Surf. Sci.* **440** 407-419 (1999).
21. Yagi, K., Minoda, H. & Degawa, M. Step bunching, step wandering and faceting self-organization at Silicon surfaces. *Surf. Sci. Rep.* **43** 45-126 (2001).
22. Jeong, H. & Williams, E. Steps on surfaces: experiment and theory. *Surf. Sci. Rep.* **34** 171-294 (1999).
23. Krug, J. & Dobbs, H. Current induced faceting of crystal surfaces. *Phys. Rev. Lett.* **73** 1947 –1950 (1994).
24. Stewart, J. & Goldenfeld, N. Spinodal decomposition of a crystal surface. *Phys. Rev. A* **46** 6505-6512 (1992).
25. Liu, F. & Metiu, H. Dynamics of phase separation of crystal surfaces. *Phys. Rev. B* **48** 5808-5817 (1993).
26. Song, S., Mochrie, S. & Stephenson, S. Faceting kinetics of stepped Si(113) surfaces: a time-resolved X-ray scattering study. *Phys. Rev. Lett.* **74** 5240-5243 (1995).
27. Song, S., Yoon, M., Mochrie, S., Stephenson, G. & Milner, S. Faceting kinetics of stepped Si(113) surfaces: dynamic scaling and nanoscale growth. *Surf. Sci.* **372** 37-63 (1997).
28. Sander, D. & Ibach, H. Surface free energy and surface stress, *Physics of covered surfaces*, in: H.Bonzel (Ed.) Landölt Bornstein New Series, **III 42,** Chap. 4, (2002).
29. An, T., Yoshimura, M., Ono, I. & Ueda, K. Elemental structure on Si(110) 16x2 revealed by STM. *Phys. Rev. B* **61** 3006-3011 (2000).
30. Song, S., Yoon, M. & Mochrie, S. Faceting, tricriticality and attractive interactions between steps in the orientational phase diagram of silicon surfaces between [113] and [5512] *Surf. Sci.* **334** 153-169 (1995).

Acknowledgements: We acknowledge J. Fuhr, G. Tréglia, and R.Kern for helpful discussions and J. P. Astier for the AFM images. Correspondence and requests for materials should be addressed to PM, muller@crmcn.univ-mrs.fr.

Figure captions:

Figure 1: Equilibrium shape and corresponding γ-plot of silicon obtained at 1373 K from a 3D silicon bulb. The surface orientations are perpendicular to the $[1\bar{1}0]$ direction[2].

Figure 2: Stereographic representation of the vicinal faces under study. **a,** Main crystallographic faces and definition of the directions $\hat{n}$ (normal vector), $\hat{\tau}$ (zone axis) and $\hat{\omega} = \hat{t} \wedge \hat{n}$ of a crystalline face. **b,** normal vectors to the vicinal faces (red) and their corresponding closest stable faces (blue).

Figure 3: AFM image of a hill-and-valley structure obtained after annealing a (118) vicinal surface in UHV conditions at 1373 K during 150 h. The facets F_1 and F_2 are (001) and (113) respectively. Geometrical data are: λ=5.5±0.2 μm, α=10±0.1 deg, β=16±2 deg, the maximum height of the "factory roof" is 0.6±0.02 μm.

Figure 4: Temporal evolution of the wavelength λ and the crystallographic angle β for all the studied vicinal faces. The angle α, which does not evolve with time, is not reported. Lines are only guides for the eyes and the error-bars correspond to experimental reproducibility.

Figure 5: Schematic representation of the mechanism of kinetic faceting. *t* represents the time.

Figure 6: **Surface stress polar dependence**. In units of $\sqrt{\frac{E\rho}{1-\nu^2}}$ calculated for the (100) face.

Table caption:

Table I: Decomposition of the vicinal faces in F_1 and F_2 facets for the stationary state.

Figure 1

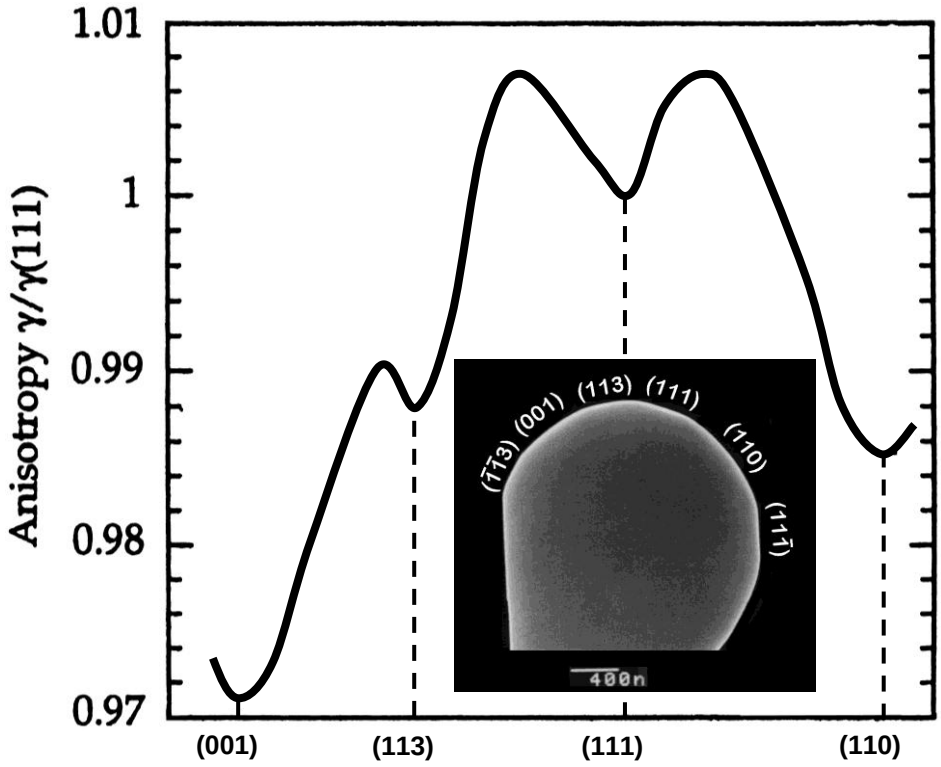
1.01
1
0.99
0.98
0.97
Anisotropy γ/γ(111)
(001)
(113)
(111)
(110)
(1̄1̄3) (001) (113) (111) (110) (11̄1)
400n

Figure 2

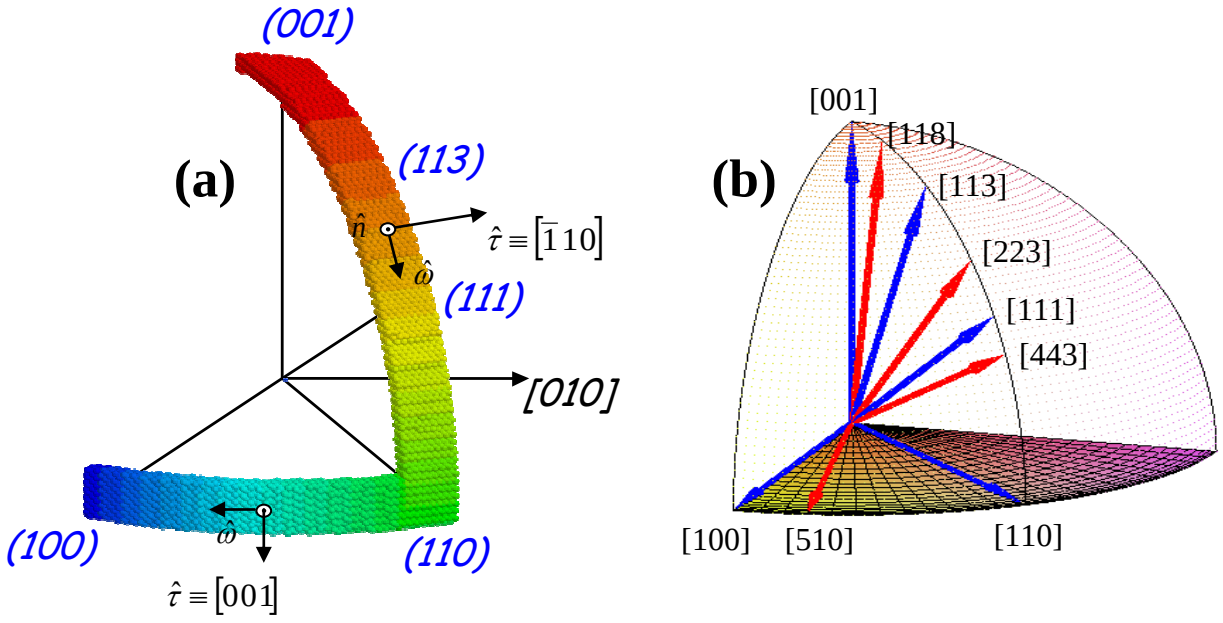
(a)
(001)
(113)
(111)
[010]
(100)
(110)
$\hat{n}$
$\hat{\omega}$
$\hat{\tau} \equiv [\bar{1}10]$
$\hat{\omega}$
$\hat{\tau} \equiv [001]$
(b)
[001]
[118]
[113]
[223]
[111]
[443]
[100]
[510]
[110]

Figure 3

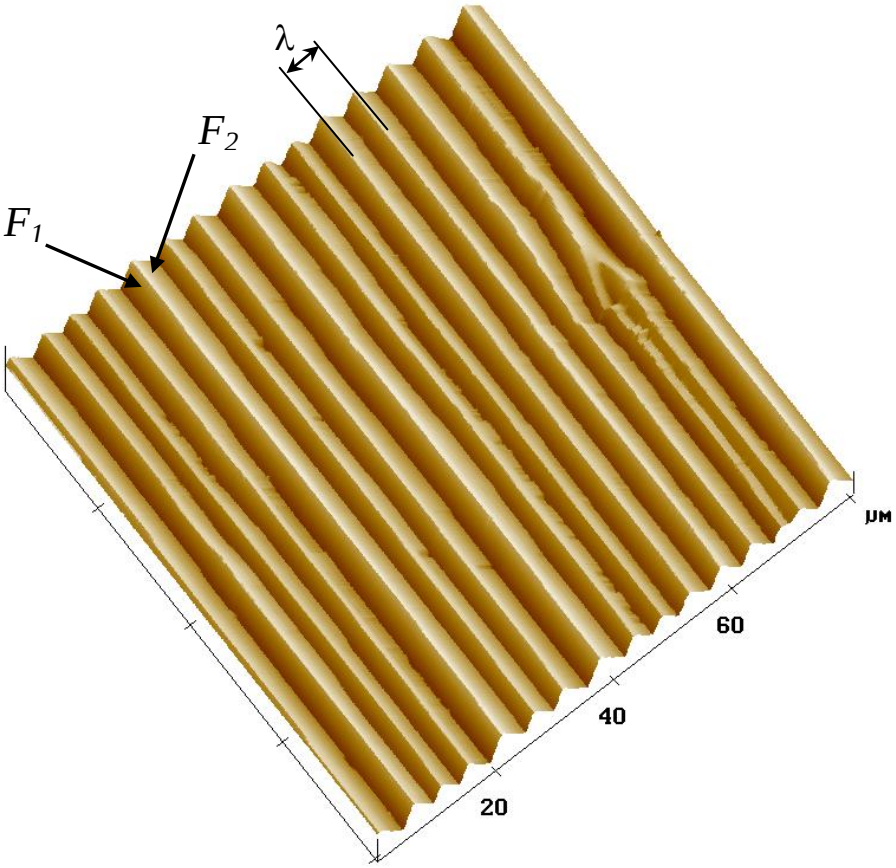

Figure 4

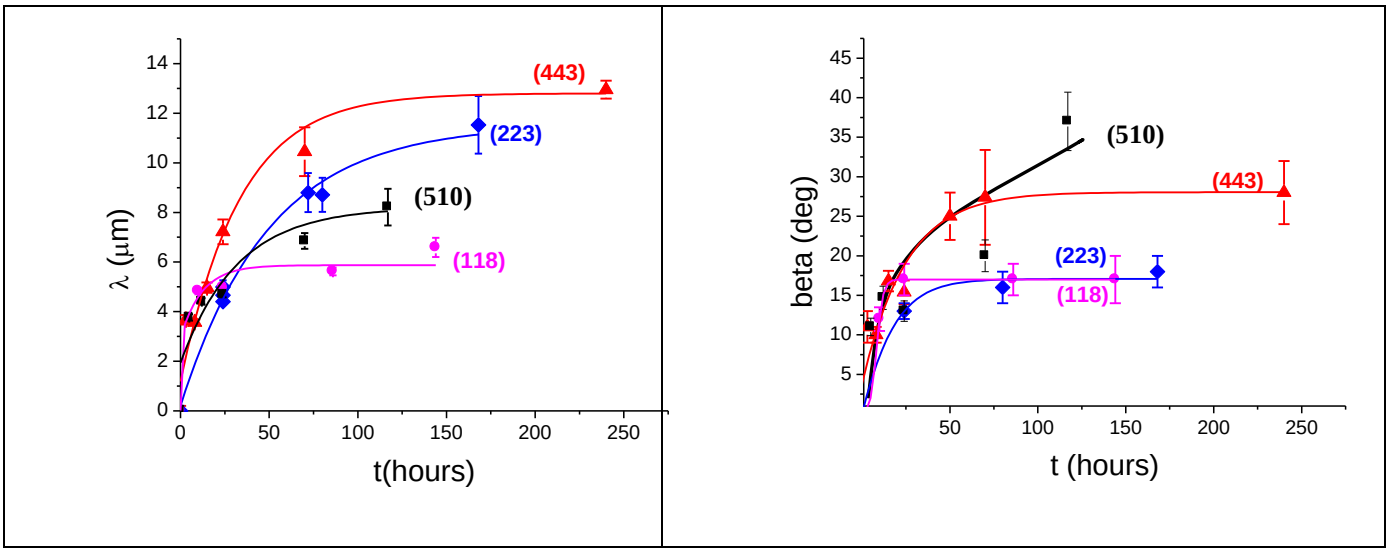

Figure 5

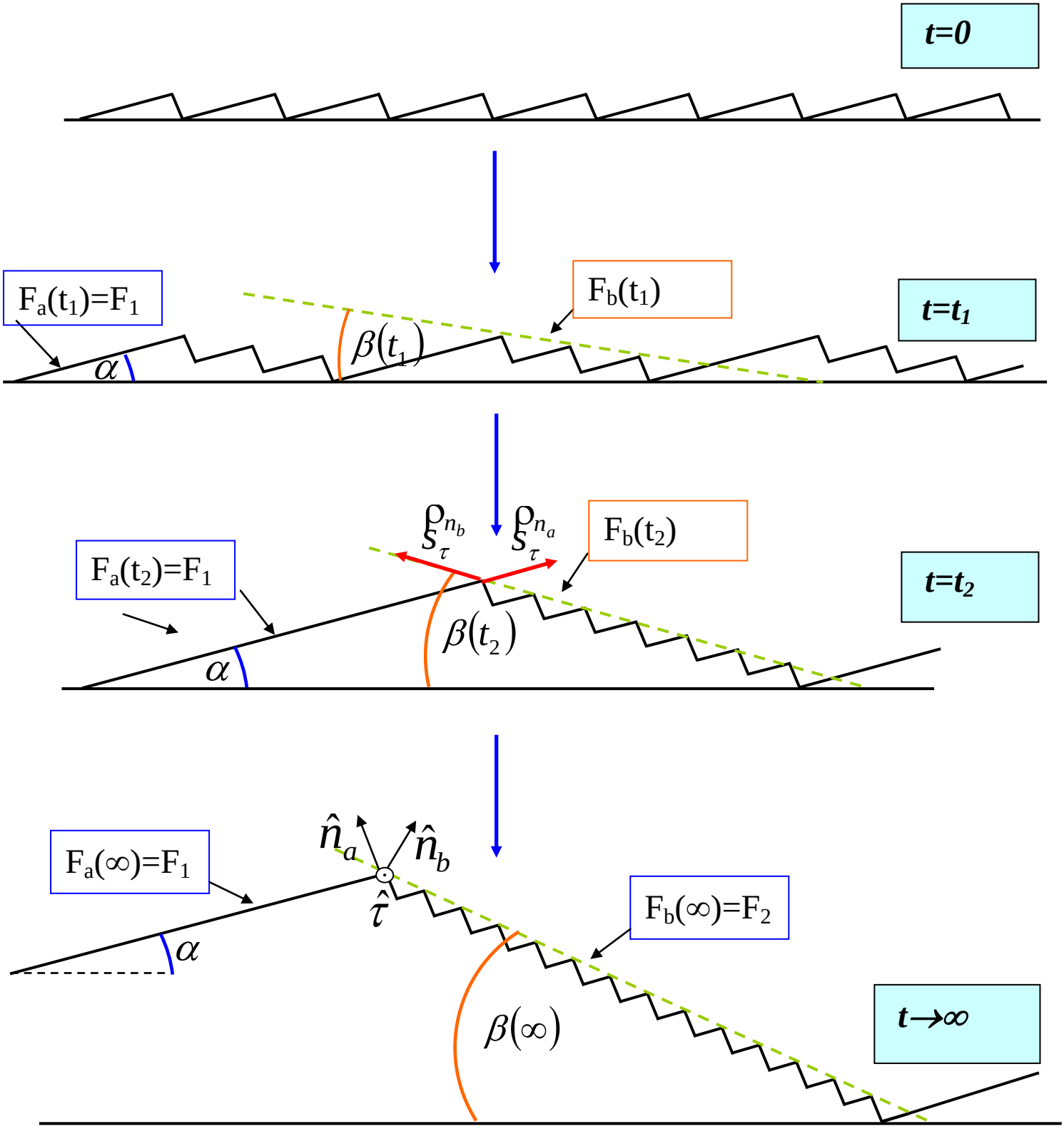
t=0
F_a(t_1)=F_1
F_b(t_1)
t=t_1
β(t_1)
α
ρ_{n_b}/S_τ
ρ_{n_a}/S_τ
F_b(t_2)
F_a(t_2)=F_1
t=t_2
β(t_2)
α
n̂_a
n̂_b
τ̂
F_a(∞)=F_1
F_b(∞)=F_2
α
β(∞)
t→∞

Figure 6

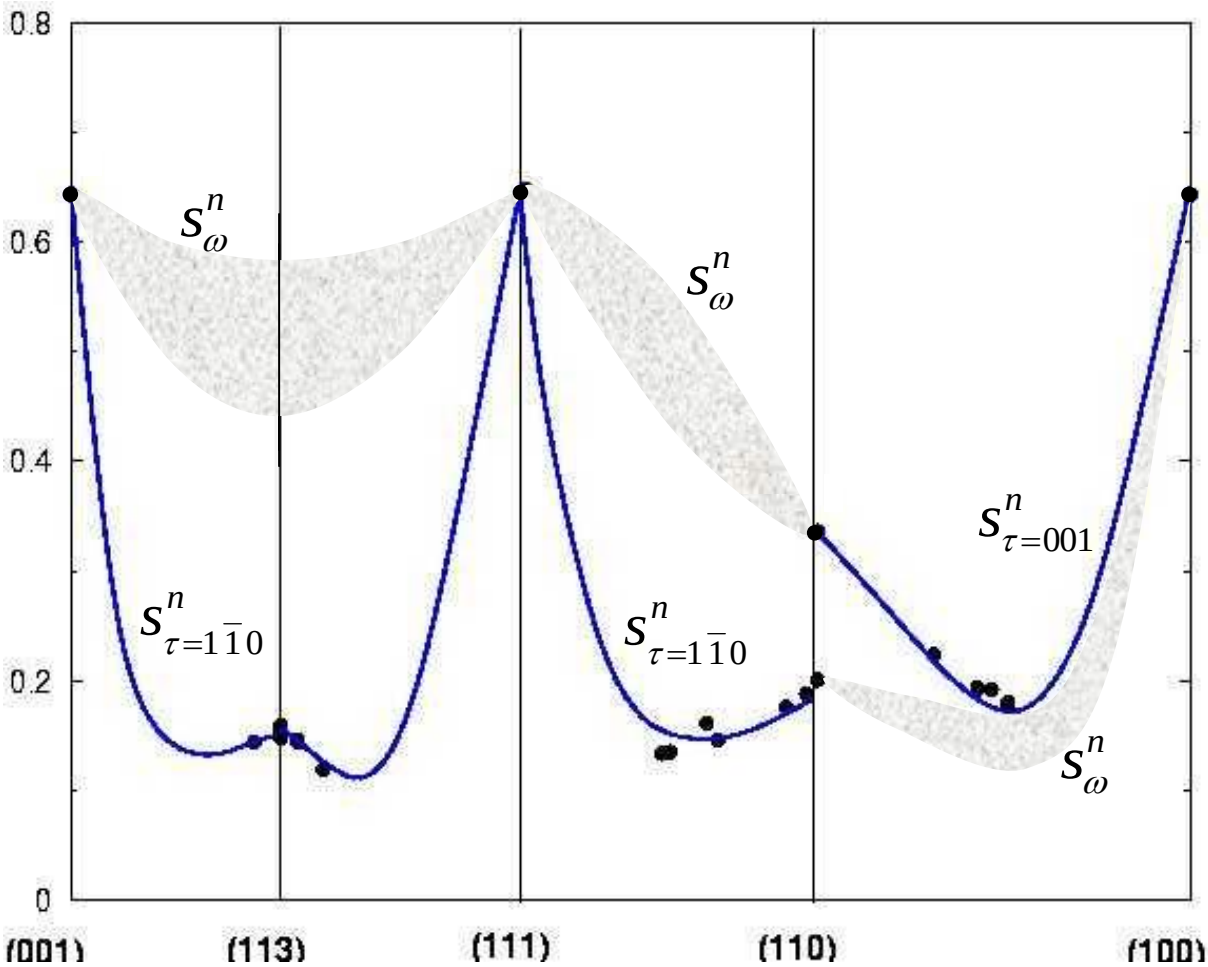
0.8
0.6
0.4
0.2
0
S^n_ω
S^n_ω
$S^n_{\tau=1\bar{1}0}$
$S^n_{\tau=1\bar{1}0}$
$S^n_{\tau=001}$
S^n_ω
(001)
(113)
(111)
(110)
(100)

Table 1

Vicinal face	**(118)**	**(223)**	**(443)**	**(510)**
F_1 (flat at the atomic scale)	(001)	(111)	(111)	(100)
F_2 (exhibit monoatomic steps)	(113)	(113)	(110)	(110)